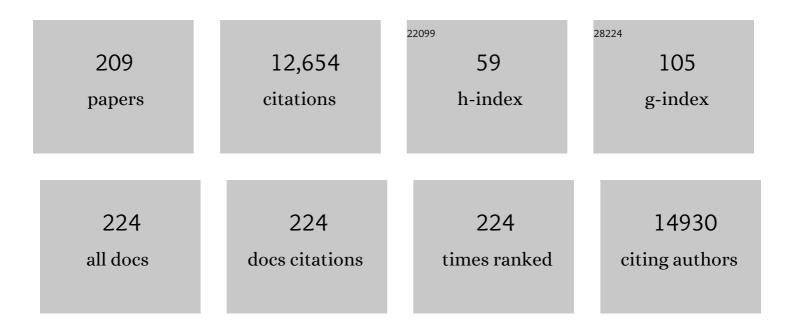
Maarten B J Roeffaers

List of Publications by Year in descending order

Source: https://exaly.com/author-pdf/757294/publications.pdf Version: 2024-02-01



#	Article	lF	CITATIONS
1	Planar heterojunction boosts solar-driven photocatalytic performance and stability of halide perovskite solar photocatalyst cell. Applied Catalysis B: Environmental, 2022, 301, 120760.	10.8	33
2	Micelle Formation inside Zeolites: A Critical Step in Zeolite Surfactant-Templating Observed by Raman Microspectroscopy. , 2022, 4, 49-54.		3
3	Metal–biomolecule frameworks (BioMOFs): a novel approach for "green―optoelectronic applications. Chemical Communications, 2022, 58, 677-680.	2.2	7
4	Spatial Heterogeneity of n-Phases Leads to Different Photophysical Properties in Quasi-Two-Dimensional Methylammonium Lead Bromide Perovskite. Journal of Physical Chemistry C, 2022, 126, 478-486.	1.5	4
5	Photocatalytic Anaerobic Oxidation of Aromatic Alcohols Coupled With H2 Production Over CsPbBr3/GO-Pt Catalysts. Frontiers in Chemistry, 2022, 10, 833784.	1.8	8
6	Metal Halide Perovskite Based Heterojunction Photocatalysts. Angewandte Chemie - International Edition, 2022, 61, .	7.2	48
7	Metal Halide Perovskite Based Heterojunction Photocatalysts. Angewandte Chemie, 2022, 134, .	1.6	11
8	S-scheme CoTiO3/Cd9.51Zn0.49S10 heterostructures for visible-light driven photocatalytic CO2 reduction. Journal of Materials Science and Technology, 2022, 124, 164-170.	5.6	83
9	Photothermal Suzuki Coupling Over a Metal Halide Perovskite/Pd Nanocube Composite Catalyst. ACS Applied Materials & Interfaces, 2022, 14, 17185-17194.	4.0	23
10	Solar Photocatalytic Oxidation of Methane to Methanol with Water over RuO _{<i>x</i>} /ZnO/CeO ₂ Nanorods. ACS Sustainable Chemistry and Engineering, 2022, 10, 16-22.	3.2	30
11	Solar-to-Chemical Fuel Conversion via Metal Halide Perovskite Solar-Driven Electrocatalysis. Journal of Physical Chemistry Letters, 2022, 13, 25-41.	2.1	10
12	Multiscale Visualization and Quantification of the Effect of Binders on the Acidity of Shaped Zeolites. ACS Catalysis, 2022, 12, 6794-6808.	5.5	9
13	Atomic-scale detection of individual lead clusters confined in Linde Type A zeolites. Nanoscale, 2022, 14, 9323-9330.	2.8	2
14	Label-free detection and size estimation of combustion-derived carbonaceous particles in a microfluidic approach. Nanoscale Advances, 2022, 4, 3272-3281.	2.2	3
15	Photocatalytic Anaerobic Dehydrogenation of Alcohols over Metal Halide Perovskites: A New Acid-Free Scheme for H ₂ Production. Journal of Physical Chemistry Letters, 2022, 13, 6559-6565.	2.1	10
16	Controlled graphite surface functionalization using contact and remote photocatalytic oxidation. Carbon, 2021, 172, 637-646.	5.4	9
17	Fluorescence-assisted real-time study of magnetically immobilized enzyme stability in a crossflow membrane bioreactor. Colloids and Surfaces A: Physicochemical and Engineering Aspects, 2021, 610, 125687.	2.3	0
18	Covalent graphite modification by low-temperature photocatalytic oxidation using a titanium dioxide thin film prepared by atomic layer deposition. Catalysis Science and Technology, 2021, 11, 6724-6731.	2.1	1

#	Article	IF	CITATIONS
19	Unique emissive behavior of combustion-derived particles under illumination with femtosecond pulsed near-infrared laser light. Nanoscale Advances, 2021, 3, 5355-5362.	2.2	6
20	Texture Formation in Polycrystalline Thin Films of Allâ€Inorganic Lead Halide Perovskite. Advanced Materials, 2021, 33, e2007224.	11.1	18
21	Visualizing light-induced dynamic structural transformations of Au clusters-based photocatalyst via in situ TEM. Nano Research, 2021, 14, 2805-2809.	5.8	24
22	Selfâ€sealing thermoplastic fluoroelastomer enables rapid fabrication of modular microreactors. Nano Select, 2021, 2, 1385-1402.	1.9	3
23	Challenges and Opportunities for CsPbBr ₃ Perovskites in Low- and High-Energy Radiation Detection. ACS Energy Letters, 2021, 6, 1290-1314.	8.8	80
24	Dual-Channel Charge Carrier Transfer in CsPbX ₃ Perovskite/W ₁₈ O ₄₉ Composites for Selective Photocatalytic Benzyl Alcohol Oxidation. ACS Applied Energy Materials, 2021, 4, 3460-3468.	2.5	19
25	Innentitelbild: Chemical Imaging of Hierarchical Porosity Formation within a Zeolite Crystal Visualized by Smallâ€Angle Xâ€Ray Scattering and Inâ€Situ Fluorescence Microscopy (Angew. Chem. 25/2021). Angewandte Chemie, 2021, 133, 13802-13802.	1.6	0
26	Experimental Evidence of Chlorideâ€Induced Trap Passivation in Lead Halide Perovskites through Single Particle Blinking Studies. Advanced Optical Materials, 2021, 9, 2002240.	3.6	8
27	Synergistic Redox Reaction for Value-Added Organic Transformation via Dual-Functional Photocatalytic Systems. ACS Catalysis, 2021, 11, 4613-4632.	5.5	69
28	Chemical Imaging of Hierarchical Porosity Formation within a Zeolite Crystal Visualized by Smallâ€Angle Xâ€Ray Scattering and Inâ€Situ Fluorescence Microscopy. Angewandte Chemie, 2021, 133, 13922-13925.	1.6	2
29	Chemical Imaging of Hierarchical Porosity Formation within a Zeolite Crystal Visualized by Smallâ€Angle Xâ€Ray Scattering and Inâ€6itu Fluorescence Microscopy. Angewandte Chemie - International Edition, 2021, 60, 13803-13806.	7.2	9
30	Label-free detection of uptake, accumulation, and translocation of diesel exhaust particles in ex vivo perfused human placenta. Journal of Nanobiotechnology, 2021, 19, 144.	4.2	13
31	Impact of Amine Additives on Perovskite Precursor Aging: A Case Study of Light-Emitting Diodes. Journal of Physical Chemistry Letters, 2021, 12, 5836-5843.	2.1	6
32	State of the Art and Prospects for Halide Perovskite Nanocrystals. ACS Nano, 2021, 15, 10775-10981.	7.3	705
33	The Holeâ€Tunneling Heterojunction of Hematiteâ€Based Photoanodes Accelerates Photosynthetic Reaction. Angewandte Chemie - International Edition, 2021, 60, 16009-16018.	7.2	37
34	All-Evaporated, All-Inorganic CsPbI ₃ Perovskite-Based Devices for Broad-Band Photodetector and Solar Cell Applications. ACS Applied Electronic Materials, 2021, 3, 3023-3033.	2.0	12
35	Tunable Luminescence from Stable Silver Nanoclusters Confined in Microporous Zeolites. Advanced Optical Materials, 2021, 9, 2100526.	3.6	12
36	The Holeâ€Tunneling Heterojunction of Hematiteâ€Based Photoanodes Accelerates Photosynthetic Reaction. Angewandte Chemie, 2021, 133, 16145-16154.	1.6	2

#	Article	IF	CITATIONS
37	Trojans That Flip the Black Phase: Impurity-Driven Stabilization and Spontaneous Strain Suppression in γ-CsPbI ₃ Perovskite. Journal of the American Chemical Society, 2021, 143, 10500-10508.	6.6	33
38	Manipulating crystallization dynamics through chelating molecules for bright perovskite emitters. Nature Communications, 2021, 12, 4831.	5.8	56
39	Ultrathin 2D/2D Ti ₃ C ₂ T _{<i>x</i>/sub>/semiconductor dual-functional photocatalysts for simultaneous imine production and H₂ evolution. Journal of Materials Chemistry A, 2021, 9, 19984-19993.}	5.2	40
40	Highly Mobile Large Polarons in Black Phase CsPbl ₃ . ACS Energy Letters, 2021, 6, 568-573.	8.8	40
41	Two-dimensional perovskites with alternating cations in the interlayer space for stable light-emitting diodes. Nanophotonics, 2021, 10, 2145-2156.	2.9	17
42	Optical encoding of luminescent carbon nanodots in confined spaces. Chemical Communications, 2021, 57, 11952-11955.	2.2	1
43	Reply to â€~Fetal side' of the placenta: Anatomical mis-annotation of carbon particle â€~transfer' across the human placenta. Nature Communications, 2021, 12, 7050.	5.8	6
44	It's a trap! On the nature of localised states and charge trapping in lead halide perovskites. Materials Horizons, 2020, 7, 397-410.	6.4	345
45	Edge stabilization in reduced-dimensional perovskites. Nature Communications, 2020, 11, 170.	5.8	147
46	Silica gel solid nanocomposite electrolytes with interfacial conductivity promotion exceeding the bulk Li-ion conductivity of the ionic liquid electrolyte filler. Science Advances, 2020, 6, eaav3400.	4.7	51
47	Subsurface Defect Engineering in Single-Unit-Cell Bi ₂ WO ₆ Monolayers Boosts Solar-Driven Photocatalytic Performance. ACS Catalysis, 2020, 10, 1439-1443.	5.5	138
48	Highly Luminescent Metal Clusters Confined in Zeolites. Structure and Bonding, 2020, , 75-103.	1.0	5
49	Efficient Photocatalytic CO2 Reduction with MIL-100(Fe)-CsPbBr3 Composites. Catalysts, 2020, 10, 1352.	1.6	23
50	Resolving the Acid Site Distribution in Zn-Exchanged ZSM-5 with Stimulated Raman Scattering Microscopy. Catalysts, 2020, 10, 1331.	1.6	7
51	Correlating Acid Site Distribution and Catalytic Activity in Dealuminated Mordenite at the Single-Particle Level. ACS Catalysis, 2020, 10, 14801-14809.	5.5	10
52	Monitoring indoor exposure to combustion-derived particles using plants. Environmental Pollution, 2020, 266, 115261.	3.7	4
53	Incorporation of Cesium Lead Halide Perovskites into g-C ₃ N ₄ for Photocatalytic CO ₂ Reduction. ACS Omega, 2020, 5, 24495-24503.	1.6	28
54	Tuning the Structural and Optoelectronic Properties of Cs ₂ AgBiBr ₆ Doubleâ€Perovskite Single Crystals through Alkaliâ€Metal Substitution. Advanced Materials, 2020, 32, e2001878.	11.1	72

#	Article	IF	CITATIONS
55	Phase Transitions and Anion Exchange in All-Inorganic Halide Perovskites. Accounts of Materials Research, 2020, 1, 3-15.	5.9	67
56	Xâ€Rayâ€Induced Growth Dynamics of Luminescent Silver Clusters in Zeolites. Small, 2020, 16, e2002063.	5.2	14
57	Arabinoxylan, βâ€glucan and pectin in barley and malt endosperm cell walls: a microstructure study using CLSM and cryo‧EM. Plant Journal, 2020, 103, 1477-1489.	2.8	22
58	Direct Z-Scheme Heterojunction of Semicoherent FAPbBr ₃ /Bi ₂ WO ₆ Interface for Photoredox Reaction with Large Driving Force. ACS Nano, 2020, 14, 16689-16697.	7.3	167
59	Energy-Efficient Ammonia Production from Air and Water Using Electrocatalysts with Limited Faradaic Efficiency. ACS Energy Letters, 2020, 5, 1124-1127.	8.8	29
60	Solar-Driven Metal Halide Perovskite Photocatalysis: Design, Stability, and Performance. ACS Energy Letters, 2020, 5, 1107-1123.	8.8	400
61	Actomyosinâ€dependent invasion of endothelial sprouts in collagen. Cytoskeleton, 2020, 77, 261-276.	1.0	2
62	Fast quantitative time lapse displacement imaging of endothelial cell invasion. PLoS ONE, 2020, 15, e0227286.	1.1	7
63	Matrix deformations around angiogenic sprouts correlate to sprout dynamics and suggest pulling activity. Angiogenesis, 2020, 23, 315-324.	3.7	40
64	Tunable white emission of silver-sulfur-zeolites as single-phase LED phosphors. Methods and Applications in Fluorescence, 2020, 8, 024004.	1.1	9
65	Material properties determining insecticidal activity of activated carbon on the pharaoh ant (Monomorium pharaonis). Journal of Pest Science, 2019, 92, 643-652.	1.9	4
66	Single-Step Synthesis of Dual Phase Bright Blue-Green Emitting Lead Halide Perovskite Nanocrystal Thin Films. Chemistry of Materials, 2019, 31, 6824-6832.	3.2	26
67	Role of Electron–Phonon Coupling in the Thermal Evolution of Bulk Rashba-Like Spin-Split Lead Halide Perovskites Exhibiting Dual-Band Photoluminescence. ACS Energy Letters, 2019, 4, 2205-2212.	8.8	58
68	Low-temperature activation of carbon black by selective photocatalytic oxidation. Nanoscale Advances, 2019, 1, 2873-2880.	2.2	14
69	Thermal unequilibrium of strained black CsPbI ₃ thin films. Science, 2019, 365, 679-684.	6.0	444
70	Correlated super-resolution fluorescence and electron microscopy reveals the catalytically active nanorods within individual H-ZSM-22 zeolite particles. Catalysis Science and Technology, 2019, 9, 4645-4650.	2.1	10
71	Nanocarrier systems assembled from PEGylated hyperbranched poly(arylene oxindole). European Polymer Journal, 2019, 119, 247-259.	2.6	7
72	A unique recipe for glass beads at Iron Age Sardis. Journal of Archaeological Science, 2019, 108, 104974.	1.2	9

#	Article	IF	CITATIONS
73	Vaporâ€Phase Linker Exchange of the Metal–Organic Framework ZIFâ€8: A Solventâ€Free Approach to Postâ€synthetic Modification. Angewandte Chemie - International Edition, 2019, 58, 18471-18475.	7.2	42
74	Hot Ï€â€Electron Tunneling of Metal–Insulator–COF Nanostructures for Efficient Hydrogen Production. Angewandte Chemie - International Edition, 2019, 58, 18290-18294.	7.2	138
75	Vaporâ€Phase Linker Exchange of the Metal–Organic Framework ZIFâ€8: A Solventâ€Free Approach to Postâ€synthetic Modification. Angewandte Chemie, 2019, 131, 18642-18646.	1.6	14
76	Ambient black carbon particles reach the fetal side of human placenta. Nature Communications, 2019, 10, 3866.	5.8	383
77	Indirect tail states formation by thermal-induced polar fluctuations in halide perovskites. Nature Communications, 2019, 10, 484.	5.8	88
78	Crosslinked Polyvinylnorborneneâ€Based Membranes as a New Class of Solventâ€Resistant Nanofiltration Membranes. Journal of Polymer Science Part A, 2019, 57, 1593-1600.	2.5	4
79	A Titanium(IV)â€Based Metal–Organic Framework Featuring Defectâ€Rich Tiâ€O Sheets as an Oxidative Desulfurization Catalyst. Angewandte Chemie, 2019, 131, 9258-9263.	1.6	37
80	Polyvinylnorbornene Gas Separation Membranes. Polymers, 2019, 11, 704.	2.0	14
81	A Titanium(IV)â€Based Metal–Organic Framework Featuring Defectâ€Rich Tiâ€O Sheets as an Oxidative Desulfurization Catalyst. Angewandte Chemie - International Edition, 2019, 58, 9160-9165.	7.2	99
82	Tracking Structural Phase Transitions in Leadâ€Halide Perovskites by Means of Thermal Expansion. Advanced Materials, 2019, 31, e1900521.	11.1	88
83	Silver Zeolite Composite-Based LEDs: Origin of Electroluminescence and Charge Transport. ACS Applied Materials & Interfaces, 2019, 11, 12179-12183.	4.0	14
84	A Facetâ€Specific Quantum Dot Passivation Strategy for Colloid Management and Efficient Infrared Photovoltaics. Advanced Materials, 2019, 31, e1805580.	11.1	87
85	Sunny Days for Perovskite Optoelectronics. ChemNanoMat, 2019, 5, 251-252.	1.5	0
86	Active Role of Methanol in Post-Synthetic Linker Exchange in the Metal–Organic Framework UiO-66. Chemistry of Materials, 2019, 31, 1359-1369.	3.2	43
87	Structural and Photophysical Characterization of Ag Clusters in LTA Zeolites. Journal of Physical Chemistry C, 2019, 123, 10630-10638.	1.5	25
88	Luminescent silver–lithium-zeolite phosphors for near-ultraviolet LED applications. Journal of Materials Chemistry C, 2019, 7, 14366-14374.	2.7	17
89	C(sp ³)–H Bond Activation by Perovskite Solar Photocatalyst Cell. ACS Energy Letters, 2019, 4, 203-208.	8.8	114
90	Efficient and Selective Photocatalytic Oxidation of Benzylic Alcohols with Hybrid Organic–Inorganic Perovskite Materials. ACS Energy Letters, 2018, 3, 755-759.	8.8	222

#	Article	IF	CITATIONS
91	Confinement of Highly Luminescent Lead Clusters in Zeolite A. Journal of Physical Chemistry C, 2018, 122, 13953-13961.	1.5	24
92	Imaging Heterogeneously Distributed Photoâ€Active Traps in Perovskite Single Crystals. Advanced Materials, 2018, 30, e1705494.	11.1	28
93	Rapid and labelâ€free optical detection of individual carbon air pollutant nanoparticulates in biomedical samples. Journal of Biophotonics, 2018, 11, e201700233.	1.1	3
94	Resolving the Framework Position of Organic Structure-Directing Agents in Hierarchical Zeolites via Polarized Stimulated Raman Scattering. Journal of Physical Chemistry Letters, 2018, 9, 1778-1782.	2.1	14
95	Unravelling the Redoxâ€catalytic Behavior of Ce ⁴⁺ Metal–Organic Frameworks by Xâ€ray Absorption Spectroscopy. ChemPhysChem, 2018, 19, 373-378.	1.0	89
96	Correlating Catalyst Structure and Activity at the Nanoscale. ChemNanoMat, 2018, 4, 6-14.	1.5	12
97	Light- and Temperature-Modulated Magneto-Transport in Organic–Inorganic Lead Halide Perovskites. ACS Energy Letters, 2018, 3, 39-45.	8.8	15
98	Perovskite-Based Devices: Photophysical Pathways in Highly Sensitive Cs2 AgBiBr6 Double-Perovskite Single-Crystal X-Ray Detectors (Adv. Mater. 46/2018). Advanced Materials, 2018, 30, 1870353.	11.1	8
99	Reversible and Site-Dependent Proton-Transfer in Zeolites Uncovered at the Single-Molecule Level. Journal of the American Chemical Society, 2018, 140, 14195-14205.	6.6	22
100	Combustion-derived particles inhibit in vitro human lung fibroblast-mediated matrix remodeling. Journal of Nanobiotechnology, 2018, 16, 82.	4.2	9
101	Photophysical Pathways in Highly Sensitive Cs ₂ AgBiBr ₆ Doubleâ€Perovskite Singleâ€Crystal Xâ€Ray Detectors. Advanced Materials, 2018, 30, e1804450.	11.1	173
102	The 2018 correlative microscopy techniques roadmap. Journal Physics D: Applied Physics, 2018, 51, 443001.	1.3	99
103	Giant Electron–Phonon Coupling and Deep Conduction Band Resonance in Metal Halide Double Perovskite. ACS Nano, 2018, 12, 8081-8090.	7.3	190
104	Improving preservation state assessment of carbonate microfossils in paleontological research using label-free stimulated Raman imaging. PLoS ONE, 2018, 13, e0199695.	1.1	6
105	Highly Photoluminescent Sulfide Clusters Confined in Zeolites. Journal of Physical Chemistry C, 2018, 122, 14761-14770.	1.5	13
106	Shaping the Optical Properties of Silver Clusters Inside Zeolite A via Guest–Host–Guest Interactions. Journal of Physical Chemistry Letters, 2018, 9, 5344-5350.	2.1	28
107	Origin of the bright photoluminescence of few-atom silver clusters confined in LTA zeolites. Science, 2018, 361, 686-690.	6.0	134
108	Atomic scale reversible opto-structural switching of few atom luminescent silver clusters confined in LTA zeolites. Nanoscale, 2018, 10, 11467-11476.	2.8	40

#	Article	IF	CITATIONS
109	The power of single molecule microscopy: from nanoparticle investigations to microbiome analysis. , 2018, , .		0
110	White-light from soot: closing the gap in the diagnostic market. , 2018, , .		0
111	Facile Morphologyâ€Controlled Synthesis of Organolead Iodide Perovskite Nanocrystals Using Binary Capping Agents. ChemNanoMat, 2017, 3, 223-227.	1.5	18
112	Silver Zeolite Compositesâ€Based LEDs: A Novel Solid‣tate Lighting Approach. Advanced Functional Materials, 2017, 27, 1606411.	7.8	30
113	Alternating Current Electrophoretic Deposition for the Immobilization of Antimicrobial Agents on Titanium Implant Surfaces. ACS Applied Materials & Interfaces, 2017, 9, 8533-8546.	4.0	21
114	Probing the Influence of SSZâ€13 Zeolite Pore Hierarchy in Methanolâ€toâ€Olefins Catalysis by Using Nanometer Accuracy by Stochastic Chemical Reactions Fluorescence Microscopy and Positron Emission Profiling. ChemCatChem, 2017, 9, 3470-3477.	1.8	19
115	Photopatterning of fluorescent host–guest carriers through pore activation of metal–organic framework single crystals. Chemical Communications, 2017, 53, 7222-7225.	2.2	12
116	Superconducting Ferromagnetic Nanodiamond. ACS Nano, 2017, 11, 5358-5366.	7.3	25
117	3D full-field quantification of cell-induced large deformations in fibrillar biomaterials by combining non-rigid image registration with label-free second harmonic generation. Biomaterials, 2017, 136, 86-97.	5.7	24
118	Rationalizing Acid Zeolite Performance on the Nanoscale by Correlative Fluorescence and Electron Microscopy. ACS Catalysis, 2017, 7, 5234-5242.	5.5	19
119	Solvent Polarity-Induced Pore Selectivity in H-ZSM-5 Catalysis. ACS Catalysis, 2017, 7, 4248-4252.	5.5	24
120	Label-free carbon particulates detection in bio (medical) settings (Conference Presentation). , 2017, , .		0
121	Assessing Inter and Intraâ€particle Heterogeneity in Aluminaâ€poor Hâ€ZSMâ€5 Zeolites. ChemCatChem, 2017, 3440-3445.	9, 1.8	12
122	Surface acid–base catalytic activity of ZIF-8 revealed by super-resolution fluorescence microscopy. CrystEngComm, 2017, 19, 4162-4165.	1.3	20
123	Parts per Million Detection of Alcohol Vapors via Metal Organic Framework Functionalized Surface Plasmon Resonance Sensors. Analytical Chemistry, 2017, 89, 4480-4487.	3.2	40
124	Facet-Dependent Photoreduction on Single ZnO Crystals. Journal of Physical Chemistry Letters, 2017, 8, 340-346.	2.1	42
125	Single-Molecule Fluorescence Microscopy Reveals Local Diffusion Coefficients in the Pore Network of an Individual Catalyst Particle. Journal of the American Chemical Society, 2017, 139, 13632-13635.	6.6	70
126	Form Follows Function: Warming White LEDs Using Metal Cluster-Loaded Zeolites as Phosphors. ACS Energy Letters, 2017, 2, 2491-2497.	8.8	25

#	Article	IF	CITATIONS
127	Silver Clusters in Zeolites: From Self-Assembly to Ground-Breaking Luminescent Properties. Accounts of Chemical Research, 2017, 50, 2353-2361.	7.6	72
128	Direct Laser Writing of δ- to α-Phase Transformation in Formamidinium Lead Iodide. ACS Nano, 2017, 11, 8072-8083.	7.3	66
129	Highly controllable direct femtosecond laser writing of gold nanostructures on titanium dioxide surfaces. Nanoscale, 2017, 9, 13025-13033.	2.8	7
130	Adsorption and Separation of Aromatic Amino Acids from Aqueous Solutions Using Metal–Organic Frameworks. ACS Applied Materials & Interfaces, 2017, 9, 30064-30073.	4.0	35
131	Origin and Abatement of Heterogeneity at the Support Granule Scale of Silver on Silica Catalysts. ChemCatChem, 2017, 9, 4562-4569.	1.8	11
132	Children's Urinary Environmental Carbon Load. A Novel Marker Reflecting Residential Ambient Air Pollution Exposure?. American Journal of Respiratory and Critical Care Medicine, 2017, 196, 873-881.	2.5	94
133	Photocatalysis assisted simultaneous carbon oxidation and NOx reduction. Applied Catalysis B: Environmental, 2017, 202, 381-387.	10.8	21
134	Fibrin structural and diffusional analysis suggests that fibers are permeable to solute transport. Acta Biomaterialia, 2017, 47, 25-39.	4.1	23
135	Zr-Based MOF-808 as Meerwein–Ponndorf–Verley Reduction Catalyst for Challenging Carbonyl Compounds. Catalysts, 2016, 6, 104.	1.6	52
136	Assessing Photocatalytic Activity at the Nanoscale Using Integrated Optical and Electron Microscopy. Particle and Particle Systems Characterization, 2016, 33, 412-418.	1.2	14
137	Development and applications of nonlinear optical spectroscopy: 14th ECONOS/34th ECW meeting in Leuven (Belgium). Journal of Raman Spectroscopy, 2016, 47, 1109-1110.	1.2	1
138	Silver-induced reconstruction of an adeninate-based metal–organic framework for encapsulation of luminescent adenine-stabilized silver clusters. Journal of Materials Chemistry C, 2016, 4, 4259-4268.	2.7	22
139	Biocompatible Label-Free Detection of Carbon Black Particles by Femtosecond Pulsed Laser Microscopy. Nano Letters, 2016, 16, 3173-3178.	4.5	44
140	Single Molecule Nanospectroscopy Visualizes Proton-Transfer Processes within a Zeolite Crystal. Journal of the American Chemical Society, 2016, 138, 13586-13596.	6.6	71
141	Photoluminescence Blinking of Single-Crystal Methylammonium Lead Iodide Perovskite Nanorods Induced by Surface Traps. ACS Omega, 2016, 1, 148-159.	1.6	76
142	Direct Observation of Luminescent Silver Clusters Confined in Faujasite Zeolites. ACS Nano, 2016, 10, 7604-7611.	7.3	58
143	Nanostructured Ag-zeolite Composites as Luminescence-based Humidity Sensors. Journal of Visualized Experiments, 2016, , .	0.2	4
144	Chemoselective reduction of α,β-unsaturated carbonyl compounds with UiO-66 materials. Journal of Catalysis, 2016, 340, 136-143.	3.1	66

#	Article	IF	CITATIONS
145	Tuning the energetics and tailoring the optical properties of silver clusters confined in zeolites. Nature Materials, 2016, 15, 1017-1022.	13.3	153
146	Degradation of Methylammonium Lead Iodide Perovskite Structures through Light and Electron Beam Driven Ion Migration. Journal of Physical Chemistry Letters, 2016, 7, 561-566.	2.1	234
147	Photocatalysts in close-up. Nature, 2016, 530, 36-37.	13.7	13
148	Noninvasive Nanoscopy Uncovers the Impact of the Hierarchical Porous Structure on the Catalytic Activity of Single Dealuminated Mordenite Crystals. ChemCatChem, 2015, 7, 3646-3650.	1.8	35
149	Thermally activated LTA(Li)–Ag zeolites with water-responsive photoluminescence properties. Journal of Materials Chemistry C, 2015, 3, 11857-11867.	2.7	70
150	Highâ€Resolution Singleâ€Molecule Fluorescence Imaging of Zeolite Aggregates within Realâ€Life Fluid Catalytic Cracking Particles. Angewandte Chemie - International Edition, 2015, 54, 1836-1840.	7.2	85
151	Visualization of molecular fluorescence point spread functions via remote excitation switching fluorescence microscopy. Nature Communications, 2015, 6, 6287.	5.8	58
152	Quantitative 3D Fluorescence Imaging of Single Catalytic Turnovers Reveals Spatiotemporal Gradients in Reactivity of Zeolite H-ZSM-5 Crystals upon Steaming. Journal of the American Chemical Society, 2015, 137, 6559-6568.	6.6	69
153	Resolving Interparticle Heterogeneities in Composition and Hydrogenation Performance between Individual Supported Silver on Silica Catalysts. ACS Catalysis, 2015, 5, 6690-6695.	5.5	22
154	Reshaping anisotropic gold nanoparticles through oxidative etching: the role of the surfactant and nanoparticle surface curvature. RSC Advances, 2015, 5, 6829-6833.	1.7	28
155	Photocatalytic carbon oxidation with nitric oxide. Applied Catalysis B: Environmental, 2015, 166-167, 374-380.	10.8	10
156	Remote excitation fluorescence correlation spectroscopy using silver nanowires. Proceedings of SPIE, 2014, , .	0.8	0
157	Single molecule methods for the study of catalysis: from enzymes to heterogeneous catalysts. Chemical Society Reviews, 2014, 43, 990-1006.	18.7	115
158	X-ray irradiation-induced formation of luminescent silver clusters in nanoporous matrices. Chemical Communications, 2014, 50, 1350-1352.	2.2	49
159	Rationalizing Inter- and Intracrystal Heterogeneities in Dealuminated Acid Mordenite Zeolites by Stimulated Raman Scattering Microscopy Correlated with Super-resolution Fluorescence Microscopy. ACS Nano, 2014, 8, 12650-12659.	7.3	43
160	Delayed electron–hole pair recombination in iron(<scp>iii</scp>)-oxo metal–organic frameworks. Physical Chemistry Chemical Physics, 2014, 16, 5044-5047.	1.3	46
161	Air-based photoelectrochemical cell capturing water molecules from ambient air for hydrogen production. RSC Advances, 2014, 4, 29286-29290.	1.7	45
162	Reporter cell activity within hydrogel constructs quantified from oxygen-independent bioluminescence. Biomaterials, 2014, 35, 8065-8077.	5.7	4

#	Article	IF	CITATIONS
163	Base catalytic activity of alkaline earth MOFs: a (micro)spectroscopic study of active site formation by the controlled transformation of structural anions. Chemical Science, 2014, 5, 4517-4524.	3.7	58
164	Intergrowth of Components and Ramps in Coffin-Shaped ZSM-5 Zeolite Crystals Unraveled by Focused Ion Beam-Assisted Transmission Electron Microscopy. Microscopy and Microanalysis, 2014, 20, 42-49.	0.2	9
165	A Causal Relation between Bioluminescence and Oxygen to Quantify the Cell Niche. PLoS ONE, 2014, 9, e97572.	1.1	15
166	Iron(III)-Based Metal–Organic Frameworks As Visible Light Photocatalysts. Journal of the American Chemical Society, 2013, 135, 14488-14491.	6.6	502
167	Threeâ€Ðimensional Visualization of Defects Formed during the Synthesis of Metal–Organic Frameworks: A Fluorescence Microscopy Study. Angewandte Chemie - International Edition, 2013, 52, 401-405.	7.2	121
168	Determination and Optimization of the Luminescence External Quantum Efficiency of Silver-Clusters Zeolite Composites. Journal of Physical Chemistry C, 2013, 117, 6998-7004.	1.5	64
169	Fluorescent oxygen sensitive microbead incorporation for measuring oxygen tension in cell aggregates. Biomaterials, 2013, 34, 922-929.	5.7	24
170	Structural and Optical Properties of ZnWO ₄ :Er ³⁺ Crystals. Journal of Spectroscopy, 2013, 2013, 1-5.	0.6	8
171	Photocatalytic growth of dendritic silver nanostructures as SERS substrates. Chemical Communications, 2012, 48, 1559-1561.	2.2	38
172	Selective photocatalytic oxidation of gaseous ammonia to dinitrogen in a continuous flow reactor. Catalysis Science and Technology, 2012, 2, 1802.	2.1	13
173	Small molecule perimeter defense in entomopathogenic bacteria. Proceedings of the National Academy of Sciences of the United States of America, 2012, 109, 10821-10826.	3.3	165
174	Labelâ€Free Live ell Imaging of Nucleic Acids Using Stimulated Raman Scattering Microscopy. ChemPhysChem, 2012, 13, 1054-1059.	1.0	133
175	Optical Heterodyne-Detected Raman-Induced Kerr Effect (OHD-RIKE) Microscopy. Journal of Physical Chemistry B, 2011, 115, 5574-5581.	1.2	37
176	Molecular organization of hydrophobic molecules and co-adsorbed water in SBA-15 ordered mesoporous silica material. Physical Chemistry Chemical Physics, 2011, 13, 2706-2713.	1.3	40
177	<i>>p</i> -Xylene-Selective Metal–Organic Frameworks: A Case of Topology-Directed Selectivity. Journal of the American Chemical Society, 2011, 133, 18526-18529.	6.6	159
178	Label-free imaging of biomolecules in food products using stimulated Raman microscopy. Journal of Biomedical Optics, 2011, 16, 021118.	1.4	41
179	Interfacial synthesis of hollow metal–organic framework capsules demonstrating selective permeability. Nature Chemistry, 2011, 3, 382-387.	6.6	483
180	Single-molecule light absorption. Nature Photonics, 2011, 5, 80-81.	15.6	5

#	Article	IF	CITATIONS
181	Exploration of Atmospheric Pressure Plasma Nanofilm Technology for Straightforward Bioâ€Active Coating Deposition: Enzymes, Plasmas and Polymers, an Elegant Synergy. Plasma Processes and Polymers, 2011, 8, 965-974.	1.6	61
182	Metal–Organic Framework Single Crystals as Photoactive Matrices for the Generation of Metallic Microstructures. Advanced Materials, 2011, 23, 1788-1791.	11.1	100
183	Label-free imaging of biomolecules in food products using stimulated Raman microscopy. Journal of Biomedical Optics, 2011, 16, 021118.	1.4	7
184	Fluorescence micro(spectro)scopy as a tool to study catalytic materials in action. Chemical Society Reviews, 2010, 39, 4703.	18.7	150
185	In Situ Observation of the Emission Characteristics of Zeoliteâ€Hosted Silver Species During Heat Treatment. ChemPhysChem, 2010, 11, 1627-1631.	1.0	52
186	Optical Encoding of Silver Zeolite Microcarriers. Advanced Materials, 2010, 22, 957-960.	11.1	115
187	Highâ€Resolution Singleâ€Turnover Mapping Reveals Intraparticle Diffusion Limitation in Tiâ€MCMâ€41â€Catalyzed Epoxidation. Angewandte Chemie - International Edition, 2010, 49, 908-911.	7.2	128
188	The influence of diffusion phenomena on catalysis: A study at the single particle level using fluorescence microscopy. Catalysis Today, 2010, 157, 236-242.	2.2	29
189	A non-invasive fluorescent staining procedure allows Confocal Laser Scanning Microscopy based imaging of Mycobacterium in multispecies biofilms colonizing and degrading polycyclic aromatic hydrocarbons. Journal of Microbiological Methods, 2010, 83, 317-325.	0.7	22
190	Watching Individual Enzymes at Work. Springer Series in Chemical Physics, 2010, , 495-511.	0.2	2
191	A Critical Assessment of the Synthesis of Diameter and Chirality Controlled CNTs in Zeolites. ECS Transactions, 2009, 19, 161-174.	0.3	2
192	Superâ€Resolution Reactivity Mapping of Nanostructured Catalyst Particles. Angewandte Chemie - International Edition, 2009, 48, 9285-9289.	7.2	175
193	Characterization of Fluorescence in Heat-Treated Silver-Exchanged Zeolites. Journal of the American Chemical Society, 2009, 131, 3049-3056.	6.6	170
194	Towards direct monitoring of discrete events in a catalytic cycle at the single molecule level. Photochemical and Photobiological Sciences, 2009, 8, 453-456.	1.6	40
195	Protein Immobilization Using Atmosphericâ€Pressure Dielectricâ€Barrier Discharges: A Route to a Straightforward Manufacture of Bioactive Films. Plasma Processes and Polymers, 2008, 5, 186-191.	1.6	49
196	Photoactivation of Silverâ€Exchanged Zeoliteâ€A. Angewandte Chemie - International Edition, 2008, 47, 2813-2816.	7.2	95
197	Morphology of Large ZSM-5 Crystals Unraveled by Fluorescence Microscopy. Journal of the American Chemical Society, 2008, 130, 5763-5772.	6.6	147
198	Exploration of Single Molecule Events in a Haloperoxidase and Its Biomimic: Localization of Halogenation Activity. Journal of the American Chemical Society, 2008, 130, 13192-13193.	6.6	57

#	Article	IF	CITATIONS
199	Relating Pore Structure to Activity at the Subcrystal Level for ZSM-5: An Electron Backscattering Diffraction and Fluorescence Microscopy Study. Journal of the American Chemical Society, 2008, 130, 13516-13517.	6.6	62
200	In situ filming of reactions inside individual zeolite crystals using fluorescence microscopy. Studies in Surface Science and Catalysis, 2007, , 717-723.	1.5	3
201	Single-molecule fluorescence spectroscopy in (bio)catalysis. Proceedings of the National Academy of Sciences of the United States of America, 2007, 104, 12603-12609.	3.3	138
202	Subdiffraction Imaging through the Selective Donut-Mode Depletion of Thermally Stable Photoswitchable Fluorophores:  Numerical Analysis and Application to the Fluorescent Protein Dronpa. Journal of the American Chemical Society, 2007, 129, 16132-16141.	6.6	130
203	Dynamic Disorder and Stepwise Deactivation in a Chymotrypsin Catalyzed Hydrolysis Reaction. Journal of the American Chemical Society, 2007, 129, 15458-15459.	6.6	61
204	Space- and Time-Resolved Visualization of Acid Catalysis in ZSM-5 Crystals by Fluorescence Microscopy. Angewandte Chemie - International Edition, 2007, 46, 1706-1709.	7.2	119
205	Fluorescence microscopy: Bridging the phase gap in catalysis. Catalysis Today, 2007, 126, 44-53.	2.2	52
206	Spatially resolved observation of crystal-face-dependent catalysis by single turnover counting. Nature, 2006, 439, 572-575.	13.7	434
207	In Situ Space- and Time-Resolved Sorption Kinetics of Anionic Dyes on Individual LDH Crystals. ChemPhysChem, 2005, 6, 2295-2299.	1.0	52
208	Reactions at the Single-Molecule Level. , 0, , 281-308.		0
209	Optimized colloidal growth of hexagonal close-packed Ag microparticles and their stability under catalytic conditions. New Journal of Chemistry, 0, , .	1.4	1